

Spherical cloaking using nonlinear transformations for improved segmentation into concentric isotropic coatings

Cheng-Wei Qiu^{1,2}, Li Hu², Baile Zhang¹, Bae-Ian Wu¹, Steven G. Johnson³, and John D. Joannopoulos¹

¹*Research Laboratory of Electronics, Massachusetts Institute of Technology, Cambridge, Massachusetts 02139, USA*
cwq@mit.edu

²*Department of Electrical and Computer Engineering, National University of Singapore, 4 Engineering Drive 3, Singapore 117576.*

³*Department of Mathematics, Massachusetts Institute of Technology, Cambridge, Massachusetts 02139, USA*
stevenj@math.mit.edu

Abstract: Two novel classes of spherical invisibility cloaks based on nonlinear transformation have been studied. The cloaking characteristics are presented by segmenting the nonlinear transformation based spherical cloak into concentric isotropic homogeneous coatings. Detailed investigations of the optimal discretization (e.g., thickness control of each layer, nonlinear factor, etc.) are presented for both linear and nonlinear spherical cloaks and their effects on invisibility performance are also discussed. The cloaking properties and our choice of optimal segmentation are verified by the numerical simulation of not only near-field electric-field distribution but also the far-field radar cross section (RCS).

© 2018 Optical Society of America

OCIS codes: (290.5839) Scattering, invisibility; (160.1190) Materials: Anisotropic optical materials; (230.3205) Invisibility cloaks

References and links

1. J. B. Pendry, D. Schurig, and D. R. Smith, "Controlling electromagnetic fields," *Science* **312**, 1780 (2006).
2. D. Schurig, J. B. Pendry, and D. R. Smith, "Calculation of material properties and ray tracing in transformation media," *Opt. Express* **14**, 9794-9804 (2006). U. Leonhardt,
3. U. Leonhardt, "Optical conformal mapping," *Science* **312**, 1777-1780 (2006).
4. D. Schurig, J. B. Pendry, and D. R. Smith, "Transformation-designed optical elements," *Opt. Express* **15**, 14772-14782 (2007).
5. A. Greenleaf, M. Lassas, and G. Uhlmann, "Anisotropic conductivities that cannot be detected by EIT," *Physiol. Meas.* **24**, 413-419 (2003).
6. H. Chen and C. T. Chan, "Acoustic cloaking in three dimensions using acoustic metamaterials," *Appl. Phys. Lett.* **91**, 183518 (2007).
7. H. Chen, B. I. Wu, B. Zhang, and J. A. Kong, "Electromagnetic Wave Interactions with a Metamaterial Cloak," *Phys. Rev. Lett.* **99**, 063903 (2007).
8. B. Zhang, H. Chen, B. I. Wu, and J. A. Kong, "Extraordinary Surface Voltage Effect in the Invisibility Cloak with an Active Device Inside," *Phys. Rev. Lett.* **100**, 063904 (2008).

9. M. Rahm, D. Schurig, D. A. Roberts, S. A. Cummer, and D. R. Smith, "Design of electromagnetic cloaks and concentrators using form-invariant coordinate transformations of Maxwell's equations," *Photonics Nanostruc. Fundam. Appl.* **6**, 87 (2008).
 10. D. Kwon and D. H. Werner, "Two-dimensional eccentric elliptic electromagnetic cloaks," *Appl. Phys. Lett.* **92**, 013505 (2008).
 11. W. X. Jiang, T. J. Cui, G. X. Yu, X. Q. Lin, Q. Cheng and J. Y. Chin, "Arbitrarily elliptical cylindrical invisible cloaking," *J. Phys. D: Appl. Phys.* **41**, 085504 (2008).
 12. M. Yan, Z. Chao, and M. Qiu, "Cylindrical invisibility cloak with simplified material parameters is inherently visible," *Phys. Rev. Lett.* **99**, 233901 (2007).
 13. M. Yan, Z. Chao, and M. Qiu, "Scattering characteristics of simplified cylindrical invisibility cloaks," *Opt. Express* **15**, 17772C17782 (2007).
 14. H. Ma, S. B. Qu, Z. Xu, J. Q. Zhang, B. W. Chen, and J. F. Wang, "Material parameter equation for elliptical cylindrical cloaks," *Phys. Rev. A* **77**, 013825 (2008).
 15. W. Cai, U. K. Chettiar, A. V. Kildishev, and V. M. Shalaev, "Optical cloaking with metamaterials," *Nat. Photonics* **1**, 063904 (2007).
 16. B. Zhang, H. Chen, and B. I. Wu, "Limitations of high-order transformation and incident angle on simplified invisibility cloaks," *Opt. Express* **16**, 5445-5452 (2008).
 17. D. Schurig, J. J. Mock, B. J. Justice, S. A. Cummer, J. B. Pendry, A. F. Starr, and D. R. Smith, "Metamaterial electromagnetic cloak at microwave frequencies," *Science* **314**, 977 (2006).
 18. R. Liu, C. Ji, J. J. Mock, J. Y. Chin, T. J. Cui, and D. R. Smith, "Broadband Ground-Plane Cloak," *Science* **323**, 366-369 (2009).
 19. W. X. Jiang, J. Y. Chin, Z. Li, Q. Cheng, R. Liu, and T. J. Cui, "Analytical design of conformally invisible cloaks for arbitrarily shaped objects," *Phys. Rev. E* **77**, 066607 (2008).
 20. H. Ma, S. Qu, Z. Xu, and J. Wang, "Numerical method for designing approximate cloaks with arbitrary shapes," *Phys. Rev. E* **78**, 036608 (2008).
 21. A. Nicolet, F. Zolla, and S. Guenneau, "Electromagnetic analysis of cylindrical cloaks of an arbitrary cross section," *Opt. Lett.* **33**, 1584 (2008).
 22. C. W. Qiu, L. W. Li, T. S. Yeo, and S. Zouhdi, "Scattering by rotationally symmetric anisotropic spheres: Potential formulation and parametric studies," *Phys. Rev. E* **75**, 026609 (2007).
 23. W. Cai, U. K. Chettiar, A. K. Kildishev, G. W. Milton, and V. M. Shalaev, "Non-magnetic cloak without reflection," arXiv:0707.3641v1.
 24. R. Weder, "A rigorous analysis of high-order electromagnetic invisibility cloaks," *J. Phys. A: Math. Theor.* **41**, 065207 (2008).
 25. C. W. Qiu, L. W. Li, Q. Wu, and T. S. Yeo, "Field representations in general gyrotropic media in spherical coordinates," *IEEE Antennas Wirel. Propagat. Lett.* **4**, 467-470 (2007).
 26. C. W. Qiu, S. Zouhdi, and A. Razolek, "Modified spherical wave functions with anisotropy ratio: Application to the analysis of scattering by multilayered anisotropic shells," *IEEE Trans. Antennas Propagat.* **55**, 3515-3523 (2007).
 27. J. C. E. Sten, "DC fields and analytical image solutions for a radially anisotropic spherical conductor," *IEEE Trans. Dielect. Elec. Insul.* **2**, 360-367 (1995).
 28. B. I. Popa and S. A. Cummer, "Cloaking with optimized homogeneous anisotropic layers," *Phys. Rev. A* **79**, 023806 (2009).
 29. C. W. Qiu, L. Hu, L. Gao, "Trade-off between forward and backward scatterings of Linear and Nonlinear Spherical Invisibility Cloaks," *Progress In Electromagnetics Research*, to be submitted (2009).
-

1. Introduction

The use of coordinate transformation to control electromagnetic fields [1] has been receiving extensive attention [2, 3, 4]. This approach was generalized from the cloaking of thermal conductivity [5], and was further widely applied in electromagnetics and acoustics [1, 6], which provides new ways to conceal passive/active objects [7, 8] within their interiors invisible to external illuminations. The fundamental idea is that Maxwell's equations are invariant under a coordinate transformation if the material properties (electric permittivity and magnetic permeability) are altered appropriately; i.e., a specific spatial compression is equivalent to a variation of the material parameters in flat (original) space. Cloaks in regular shapes (e.g., spherical [1], square [9], cylindrical [10], or elliptic [11]) have been proposed based on the construction of explicit transformation matrices. There are many works devoted to the investigation of 2D cylindrical/elliptic cloaks approximated by, for example, simplified material parameters or equations [12, 13, 14, 15], or designed for limited incident angles [16]. Experimental investigations of 2D

cloaks have demonstrated significant reductions in the scattering cross section, albeit for narrow bandwidths in the microwave regime and for objects at most a few wavelengths in diameter so far [17]. Broader bandwidths have been demonstrated for cloaking an object on a ground plane, but again only for a few wavelengths diameter [18]. To design irregularly shaped cloaks, both analytical [19] and numerical methods [20, 21] have been proposed. In what follows, we will confine our discussion within the area of 3D electromagnetic spherical cloaks.

Inspired by the classic spherical cloak [1] based on a linear coordinate transformation, the expressions of electromagnetic fields were explicitly presented in terms of spherical Bessel functions along the lines of Mie scattering theory [7], and it again was demonstrated that the external incident wave cannot interact with the cloaked object in a perfect spherical cloak. Linear coordinate transformations correspond to a transverse/radial permittivity ratio (*anisotropy ratio* [22]) $\epsilon_t/\epsilon_r = r^2/(r - R_1)^2$, where R_1 is the radius of the cloaked region. The subtle point of the singularity in the coordinate transformation at the inner surface of the cloak was analytically shown to correspond to surface voltages [8] in spherical cloaks, leading to an explicit physical explanation for why the wave cannot leave the cloaked region and external waves cannot enter that region. These works on spherical cloaks considered linear coordinate transformations, while more recently nonlinear (“high-order”) transformations have been considered in order to obtain more degrees of freedom in designing the material parameters [23, 24]. In this paper, we consider the utility of nonlinear coordinate transformations to improve the performance of the cloak when it is approximated (segmented) into a sequence of piecewise-homogeneous layers. If the anisotropy ratio differs from $r^2/(r - R_1)^2$, it will lead to quite complicated formulations for the field expressions, which cannot be treated by the previous method for a position-dependent anisotropy ratio [7] or by the method for a constant anisotropy ratio [25, 26]. Here, in order to study the proposed nonlinear-transformation spherical cloaks, each anisotropic cloaking shell is discretized into multiple alternating homogeneous isotropic coatings, not only for the ease of fabrication but also for the computation convenience in dealing with arbitrary anisotropy ratios.

In general, practical implementations of passive invisibility cloaks by coordinate transformation are limited by several factors, in addition to the bandwidth limitations (from material dispersion) mentioned above. First, there are fabrication imperfections and the finite size of the subwavelength components of the metamaterials. Second, there is material absorption, which is especially challenging when an extreme resonant response is required of the material in order to obtain very large or very small permittivity/permeability. Third, there is the difficulty of fabricating continuously varying anisotropic materials. In this paper, we focus only on the third issue. A common approximation for continuously varying materials is to segment them into piecewise-homogeneous layers, and we show that the choice of coordinate transformation has a significant impact upon the success of this approximation. We argue that the segmentation is best performed in virtual space rather than in the physical (transformed) coordinates. We also demonstrate that the anisotropic materials can be further approximated by a sequence of isotropic-material layers. The optimal selection of material parameters, nonlinear transformation, and segmentation (in virtual space), in order to achieve a low scattering cross section over a wide range of observation angles, is found for nonlinear spherical cloaks and verified by numerical results.

2. Preliminaries

The configuration of the spherical cloaking structure is shown in Fig. 1. The inner region ($r < R_1$) is a perfect electric conductor (PEC) and the intermediate region ($R_1 < r < R_2$) is filled by the nonlinearly transformed spherical cloak, characterized by $\bar{\epsilon}(r)$ and $\bar{\mu}(r)$, which will be discussed below. The electric field is polarized along the x axis and propagating along the z axis.

By applying the decomposition method and separation of variables [22], the equation for the

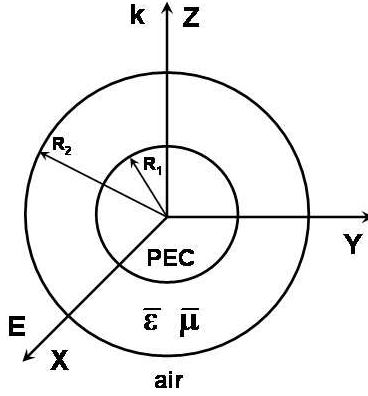


Fig. 1. The geometry of a spherical cloaking structure.

radial component of the field potentials becomes

$$\left\{ \frac{\partial^2}{\partial r^2} + \left[k_r^2 - A_{e,m} \frac{n(n+1)}{r^2} \right] \right\} f(r) = 0, \quad (1)$$

where the subscripts e and m denote the electric and magnetic anisotropic ratio, respectively, and $k_r = \omega \sqrt{\bar{\mu}_r \bar{\epsilon}_r}$ [22]. For $\bar{\epsilon}$ and $\bar{\mu}$ of perfect linear spherical cloaks [1], i.e., $A_e = A_m = r^2/(r - R_1)^2$, Eq. (1) is reduced to

$$\left\{ \frac{\partial^2}{\partial r^2} + \left[k_r^2 - \frac{n(n+1)}{(r - R_1)^2} \right] \right\} f(r) = 0. \quad (2)$$

Thus, the radial component $f(r)$ can be solved in a way similar to that for isotropic materials, except for the change in the argument of resultant Bessel/Hankel functions. However, given a set of $\bar{\epsilon}$ and $\bar{\mu}$ derived from a certain transform, the anisotropy ratio may not be $r^2/(r - R_1)^2$ anymore, and then the radial component cannot be solved explicitly in the same way. In this situation, we could approximate the original inhomogeneous anisotropic cloak by many thin, homogeneous anisotropic coatings, and the diffraction problem can thus be solved in terms of analytical Bessel/Hankel functions satisfying boundary conditions at each interface. Nevertheless, the requirement of anisotropic materials still remains. Alternatively, to further alleviate the restriction in material complexity, the original inhomogeneous anisotropic cloaking materials can be approximated by the limit of many thin, concentric, homogeneous, *isotropic* coatings, forming an effective anisotropic medium, which will be discussed in this section.

First, we consider a general spherical cloak characterized by $\bar{\epsilon} = \epsilon_r(r) \hat{r}\hat{r} + \epsilon_t(r) (\hat{\theta}\hat{\theta} + \hat{\phi}\hat{\phi})$ and $\bar{\mu} = \mu_r(r) \hat{r}\hat{r} + \mu_t(r) (\hat{\theta}\hat{\theta} + \hat{\phi}\hat{\phi})$, in which $\epsilon_r(r) = \mu_r(r)$ and $\epsilon_t(r) = \mu_t(r)$ are position-dependent in general. It is then divided into M initial-layers (anisotropic) but the thickness of individual initial layers may or may not be identical, depending on the transformation. Given a coordinate transformation function $r' = f(r)$ between the virtual space (i.e., $\Omega'(r'), 0 < r' < R_2$) and the compressed space (i.e., $\Omega(r), R_1 < r < R_2$), the stepwise segmentation in physical space (r) is desired to mimic the transformation function as well as possible and we also desire that the segmentation not be too complicated. We find that equally dividing the *virtual* space (r') into M initial-layers will make the segmentation on the physical space (r) “self-adaptive” in a simple way—it automatically uses a finer discretization in regions of physical space where the anisotropic materials are varying more rapidly—which will result in better invisibility perfor-

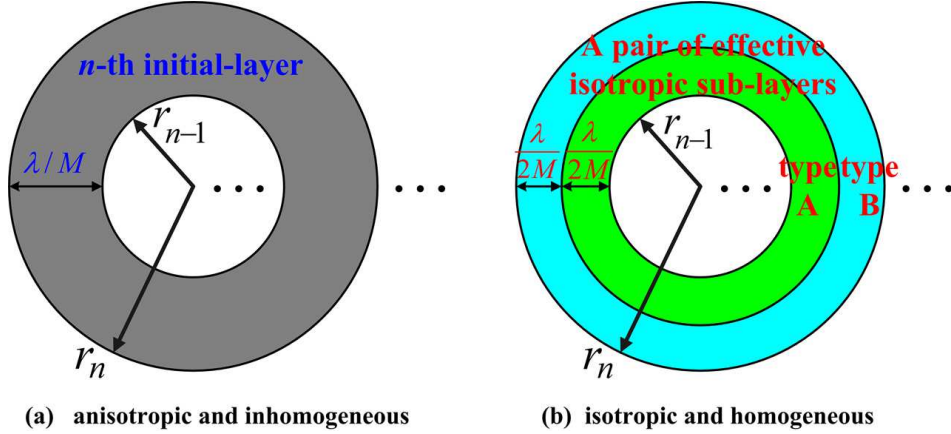


Fig. 2. The discretization of a general anisotropic spherical cloak (a) into an equivalent isotropic coated structure (b). An illustrative example for the conversion from the n -th anisotropic initial-layer (width is $r_n - r_{n-1}$) into its two sub-layers (isotropic) with equal thickness $(r_n - r_{n-1})/2$ has been shown.

mance. This conversion is illustrated in Fig. 2. Throughout this paper, we apply the same condition, i.e., the segmented layers in r' are of equal thickness, which represents a good choice of segmentation in the initial-layers in the cloak shell $R_1 < r < R_2$. By projecting the segmentation in $r'_n = R_2 \cdot n/M$ onto the physical r , one has $r_n = f^{-1}(r'_n)$, ($n=1, 2, \dots, M$). Thus, the geometry of every initial-layer in Fig. 2(a) is determined.

Subsequently, we mimic each spherically anisotropic initial layer by a pair of effective isotropic sub-layers (type-A and type-B) with equal thickness at $(r_n - r_{n-1})/2$, as shown in Fig. 2(b). The material parameters of type-A and type-B isotropic dielectrics can be inferred and derived from the result for radial conductivity by Sten [27]:

$$\epsilon_A = \mu_A = \epsilon_t + \sqrt{\epsilon_r^2 - \epsilon_t \epsilon_r} \quad (3a)$$

$$\epsilon_B = \mu_B = \epsilon_t - \sqrt{\epsilon_r^2 - \epsilon_t \epsilon_r}. \quad (3b)$$

Now, the original spherical cloak turns to be a concentric isotropic coatings. Throughout this paper, $M = 40$ and $R_2 = 2R_1 = 2\lambda$ are chosen in order that the validity of Eq. (3) can be maintained, i.e., sub-layers have to be sufficiently thin. Alternatively one could also choose a smaller M associated with the corresponding parameters determined by optimization methods and then subdivide each anisotropic layer into many more than two isotropic sub-layers.

When converting the n -th initial layer into its pair of effective isotropic sub-layers, we need to pick a specific radial position for those ϵ_r and ϵ_t on the right-hand side of Eq. (3) within the initial layer in order to determine corresponding parameters of the two isotropic dielectrics (ϵ_A, μ_A) and (ϵ_B, μ_B) on the left-hand side of Eq. (3) and in Fig. 2(b). According to [29], such a discretization mechanism using $r = r_n$ in Eq. (3) for the n -th initial layer will give a good compromise for both forward and backward scatterings, while retaining good invisibility performance.

3. Effects of Nonlinear Transformation in Nonlinear Spherical Cloaks

Pendry's spherical cloak [1] is a linear one, and hence it is a straight line if one plots the transformation function r' against the physical radius r . In what follows, we introduce two classes

of nonlinear-transformation spherical cloaks, and we discuss how to restore and improve the invisibility performance after discretization by choosing a proper nonlinear transformation and by choosing a suitable compensation scheme while discretizing the original spherical cloak into multilayer isotropic structures. The two types of spherical cloaks considered here are classified in terms of the negative (i.e., concave-down) or positive (i.e., concave-up) sign of the second derivative of the transformation function. It is important to reiterate that all three designs—linear, concave-up, and concave-down—are perfect cloaks for the exact inhomogeneous design, and we are only considering the breakdown of invisibility when the design is discretized into homogeneous layers.

3.1. Concave-Down Nonlinear Transformation

To compress a sphere of air at the radius R_2 in Ω' (original) space into a shell at the region $R_1 < r < R_2$ in Ω (compressed) space, we propose a class of prescribed functions

$$r'(x) = \frac{R_2^{x+1}}{R_2^x - R_1^x} \left[1 - \left(\frac{R_1}{r} \right)^x \right] \quad (4)$$

where x denotes the degree of the nonlinearity in the transformation. When x is very small in Eq. (4), the curves are difficult to distinguish and all approach to the same limiting case when $x \rightarrow 0$:

$$r'(x) = \frac{R_2 \text{Ln}[r/R_1]}{\text{Ln}[R_2/R_1]}. \quad (5)$$

Thus the parameters $\bar{\epsilon}$, $\bar{\mu}$ in the transformed coordinates can be written in term of $\bar{\epsilon}'$, $\bar{\mu}'$ in the original space by

$$\bar{\epsilon}(r) = A \bar{\epsilon}'(r') A^T / \det(A), \quad \bar{\mu}(r) = A \bar{\mu}'(r') A^T / \det(A) \quad (6)$$

where A is the Jacobian matrix with elements defined as $A_{ki} = \partial r_k / \partial r'_i$.

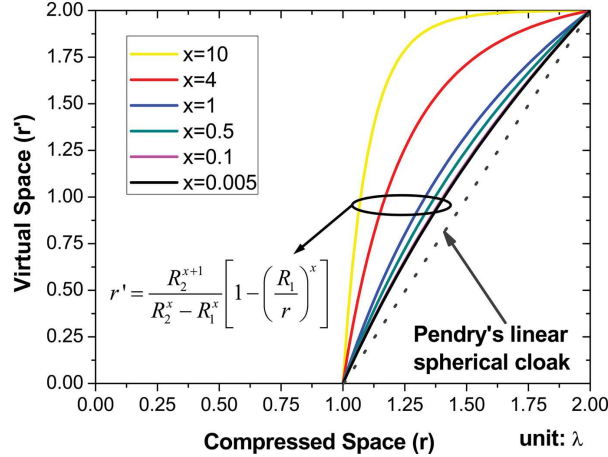


Fig. 3. The concave-down nonlinear transformation. When $x < 0.1$, all mapping curves are overlapping, meaning they effectively lead to the same performance. When x becomes large, the curve will nearly become a step function over $1\lambda < r < 2\lambda$.

Note that all curves belonging to those transformation functions in Eq. (4) have negative second derivative with respect to the physical space r , and we term this class of transformations

the *concave-down* nonlinear transformation. The nonlinear transformation function in Eq. (4) only depends on the radial component r in the spherical coordinate system (r, θ, ϕ) . Thus it is easy to find that the Jacobian matrix A is diagonal. Considering that the original space is filled with air ($\bar{\boldsymbol{\epsilon}} = \bar{\boldsymbol{\mu}} = 1$), Eq. (6) can be rewritten as

$$\bar{\boldsymbol{\epsilon}} = \bar{\boldsymbol{\mu}} = \text{diag}[\lambda_r^2, \lambda_\theta^2, \lambda_\phi^2] / \lambda_r \lambda_\theta \lambda_\phi = \text{diag}\left[\frac{\lambda_r}{\lambda_\theta \lambda_\phi}, \frac{\lambda_\theta}{\lambda_r \lambda_\phi}, \frac{\lambda_\phi}{\lambda_r \lambda_\theta}\right] \quad (7)$$

where

$$\lambda_r = \frac{\partial r}{\partial r'} = \frac{(R_2^x - R_1^x)r^{x+1}}{xR_1^x R_2^{x+1}} \quad (8a)$$

$$\lambda_\theta = \lambda_\phi = \frac{r}{r'} = \frac{(R_2^x - R_1^x)r^{x+1}}{R_2^{x+1}(r^x - R_1^x)} \quad (8b)$$

denoting three principal stretches of the Jacobian matrix. Finally, the desired parameters in the compressed space ($R_1 < r < R_2$) are shown to be

$$\epsilon_r = \mu_r = \frac{R_2^{x+1}(r^x - R_1^x)^2}{xR_1^x(R_2^x - R_1^x)r^{x+1}} \quad (9a)$$

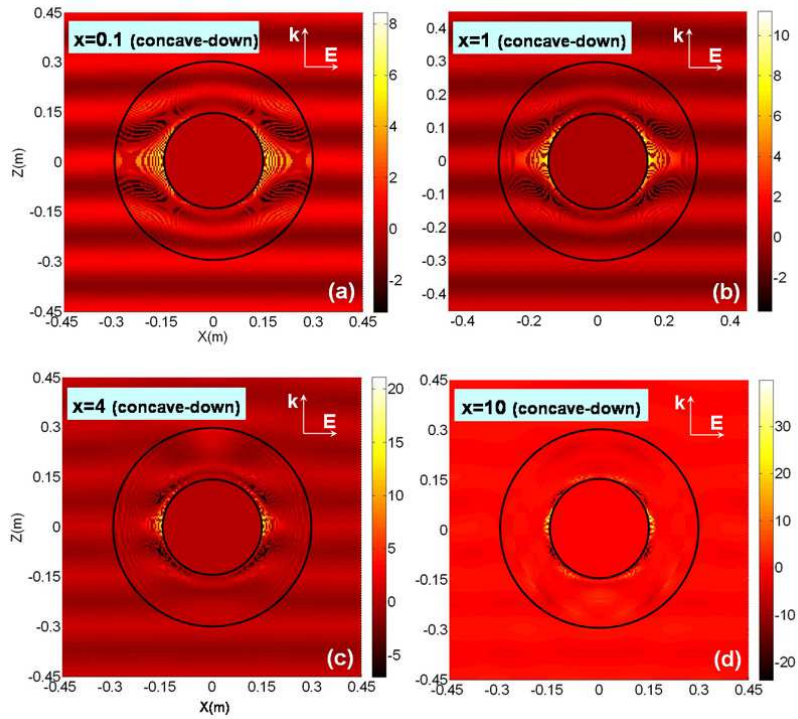
$$\epsilon_\theta = \mu_\theta = \epsilon_\phi = \mu_\phi = \frac{xR_1^x R_2^{x+1}}{(R_2^x - R_1^x)r^{x+1}}. \quad (9b)$$

Given such radial and transversal parameters, it is obvious that Eq. (1) cannot be simply solved due to the complicated anisotropy ratio $A_{e,m} = \epsilon_t / \epsilon_r = x^2 R_1^{2x} / (r^x - R_1^x)^2$ in our current case. In addition, one can also find that when the virtual space is equally discretized using a concave-down nonlinear transformation, the segmentation of the initial layers in Fig. 2 in the physical space r is

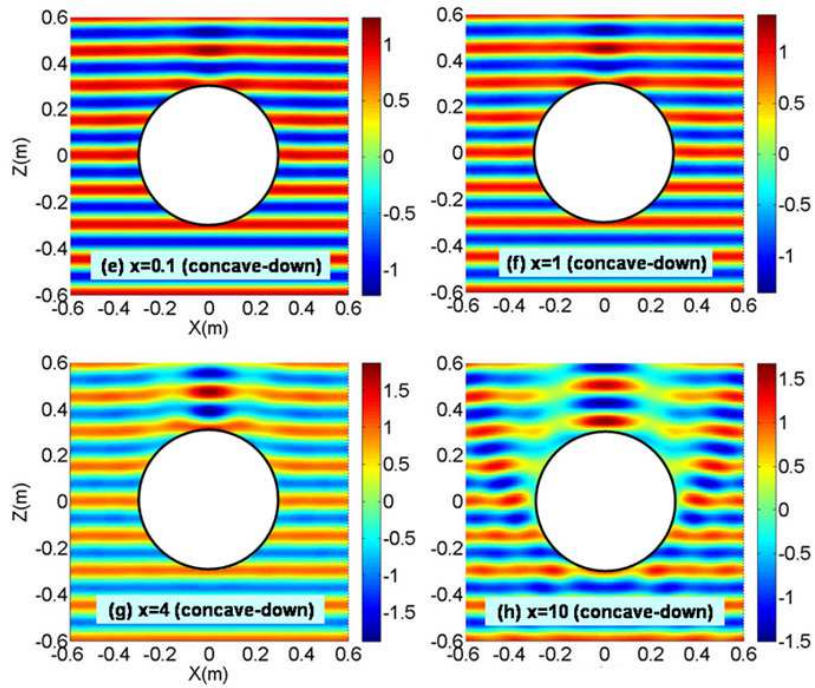
$$r_n(x) = \left[1 - \frac{R_2^x - R_1^x}{R_2^x} \frac{n}{M}\right]^{-1/x} \cdot R_1, \quad n=1, 2, \dots, M. \quad (10)$$

Here, we will study the effects of the nonlinear factor x in the near-field and far-field of the discretized nonlinear-transformation spherical cloaks. We fix $M=40$, and consider the cases of $x=0.1$, $x=1$, $x=4$, and $x=10$ in concave-down nonlinear cloaks, shown in Fig. 4. It can be seen from Figs. 4(a-d) that when x increases, the magnitude of electric field increases significantly inside the cloak. This is because more energy is guided towards the inner boundary of the PEC core, which in turn makes the cloaked PEC more *visible* to external incidences. To prove that the large electric fields only occur in the region $R_1 < r < R_2$ and to study the effect of x on individual near-field perturbations more explicitly, only the fields outside the cloak are presented in Figs. 4(e-f). One can again confirm that, for discretized concave-down nonlinear spherical cloaks, smaller x leads to smaller disturbance in electric fields in the outer space. In particular, the degradation in the invisibility in the forward direction is proportional to the value of x (see Fig. 4(g) and Fig. 4(h)).

In Fig. 5, we consider the far fields of those cases of Fig. 4. For comparison purposes, we introduce two more curves, PEC and Pendry's cloak. It should be noted that the curve corresponding to Pendry's cloak is a straight line, and the same segmentation procedure as discussed above is applied to it, which is the same as equally dividing it into M initial-layers in the physical space (see Fig. 3). From Fig. 5, it can be seen that for concave-down nonlinear transformations, the cloaking property is better retained when x is small. Except for the forward direction,



$\text{Re}[E_{\text{total}}]$ in all regions on x-z plane



$\text{Re}[E_{\text{total}}]$ outside the cloak on x-z plane

Fig. 4. Near-field interaction in the presence of the proposed nonlinear spherical cloak with different values of x for the concave-down class. The inner region $0 < r < R_1$ is filled by PEC. M is set to be 40. Frequency is 2GHz. The total electric fields are plotted only in the region $r > R_2$ in (e-h).

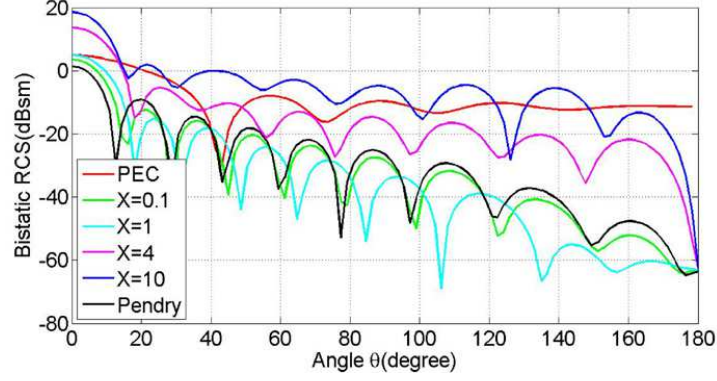


Fig. 5. Bistatic RCS of the concave-down nonlinear cloaks. $M = 40$.

concave-down nonlinear transformation with small x can achieve even lower RCS over a wide range of observation angles. As x keeps increasing, their RCSs are increasing dramatically and can be larger than that of a uncloaked PEC core (e.g., $x = 10$). No matter how large x becomes, the suppressed backward scattering is still maintained [7] though it is not exactly zero due to the discretization, but the forward scattering will become higher and higher, which is not desired in the cloaking application. Those far-field characteristics are consistent with the perturbation in corresponding near-field patterns in Fig. 4.

3.2. Concave-Up Nonlinear Transformation

We can also propose another class of prescribed functions

$$r'(x) = \frac{R_2 R_1^x}{R_2^x - R_1^x} \left[\left(\frac{r}{R_1} \right)^x - 1 \right]. \quad (11)$$

It is found that when $x \rightarrow 0$, it also approaches to the same limit as Eq. (5). In the same manner, we can obtain the desired parameters in the compressed space ($R_1 < r < R_2$)

$$\varepsilon_r = \mu_r = \frac{R_2 (r^x - R_1^x)^2}{x (R_2^x - R_1^x) r^{x+1}} \quad (12a)$$

$$\varepsilon_\theta = \mu_\theta = \varepsilon_\phi = \mu_\phi = \frac{x R_2 r^{x-1}}{R_2^x - R_1^x}. \quad (12b)$$

Note that the case $x = 1$ is exactly Pendry's linear spherical cloak.

It can be seen in Fig. 6 that all curves belonging to Eq. (11) have positive second derivatives, and we term this class of transformations as the *concave-up* nonlinear transformations. Also, it is found that the limiting case of Eq. (5), i.e., $x \rightarrow 0$, is the dividing line between the concave-down and concave-up classes. Since $x \ll 1$ in Eq. (11) is actually very close to the situation of $x \ll 1$ for concave-down nonlinear transformations, we will not revisit that case here. Instead, we only consider $x = 1$, $x = 4$, and $x = 10$ concave-up transformations [Eq. (12)], and the segmentation for concave-up nonlinear spherical cloaks in physical space r turns out to be

$$r_n(x) = \left[\frac{R_2^x - R_1^x}{R_1^x} \frac{n}{M} + 1 \right]^{1/x} \cdot R_1, \quad n=1, 2, \dots, M. \quad (13)$$

We are interested to see which class will give rise to better invisibility performance, after discretization, if all the other conditions are the same. We still plot the near field of concave-up cloaks at “ $x=1$ ”, “ $x=4$ ”, and “ $x=10$ ”. Comparing Fig. 4 with Fig. 7, one can see that: (1)

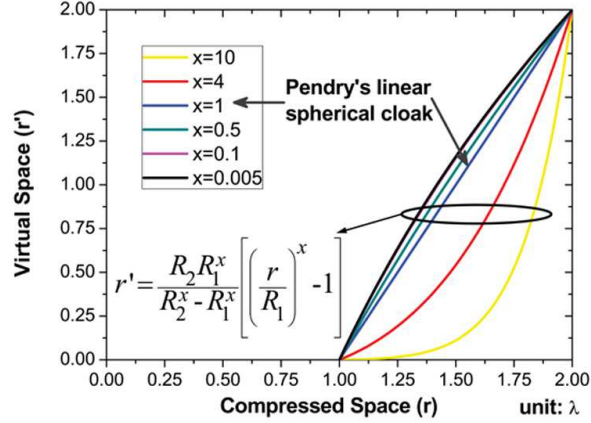


Fig. 6. The concave-up nonlinear transformation. When $x = 1$, it is exactly Pendry's linear cloak, which can be verified by inserting $x = 1$ into Eq. (12). When x gets extremely large, the mapping curve will nearly become a sharp impulse when $r \rightarrow 2\lambda$.

the peak amplitude of the electric field is proportional to x in both classes; (2) for each value of x , concave-up transformation cloaks have lower peak amplitudes than concave-down transformation cloaks, i.e., the perturbation inside the cloak region is smaller; (3) the perturbation outside the cloak of concave-up transformation cloaks is also lower than that of concave-down transformation cloaks in all cases of x ; (4) the invisibility performance is better maintained for concave-up transformations even when $x = 10$ or even larger. Hence, spherical cloaks based on concave-up nonlinear transformations exhibit better invisibility after discretization.

Fig. 8 exhibits some interesting features which distinguish it from the far fields of concave-down transformations in Fig. 5. Over a wide range of angles, the invisibility performance of spherical cloaks based on concave-up nonlinear transformations are more stable under variations in x . More importantly, when x increases (e.g., $x = 4$ or $x = 10$), though the RCS will be a bit larger than Pendry's linear cloak at most angles, the RCS near the forward direction will be reduced greatly compared with that of classic linear cloak. Such far-field phenomena are also connected with the near-field patterns. It is important to point out that the increase of x in concave-up transformations [see Figs. 7(a-c)] will push the "hot" areas (where the electric field is very high) further and further away from the spherical PEC core, so the induced shadow and the far-field pattern become stable with increasing x . However, the increase of x in the concave-down transformations has little effect in shifting away the "hot" positions from the core [see Fig. 4(a-d)], which results in larger interaction with the PEC core. Hence, the RCS reduction in the far field is degraded with the increase of x in the concave-down class as shown in Fig. 5.

4. Justification of Improved Segmentation

It has been pointed out that usually we require a large value of M during the discretization process, otherwise the conversion scheme in Fig. 2 will lose its accuracy. We also find that a nonlinear transformation with a given x of its concave-up class will yield a better invisibility by taking the segmentation as Eq. (13) in the physical space (this is also the only way to determine sub-layers of type-A and type-B dielectrics in practice). Here the justification is given. The concave-up class with $x = 4$, which is characterized by the mapping curve $r'(4) = \frac{R_2 R_1^4}{R_2^4 - R_1^4} \left[\left(\frac{r}{R_1} \right)^4 - 1 \right]$, is considered as an example.

In Table I, different segmentation $r_n(x)$ sets (see Eq. 13) for real radius r are applied to

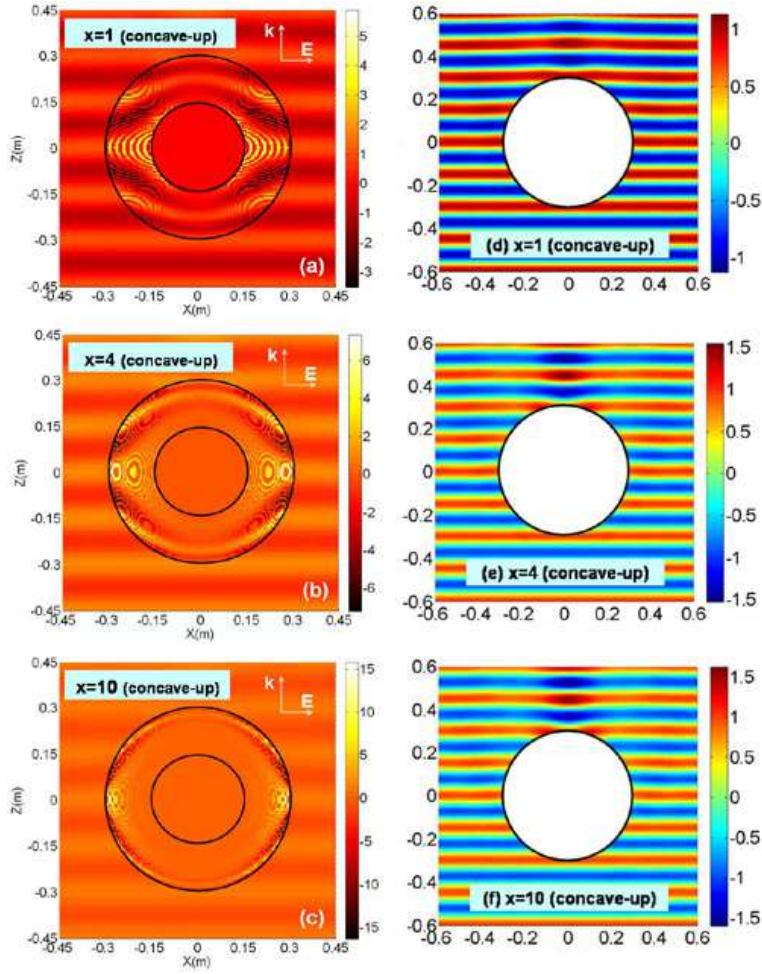


Fig. 7. $\text{Re}[E_{\text{total}}]$ on x - z plane for the proposed concave-up nonlinear transformation cloaks at $x = 1$, $x = 4$ and $x = 10$, respectively. Figs. 7(a-c) present total electric fields in all areas while Figs. 7(e-f) show the total fields only outside the cloak ($r > R_2$). $M = 40$ and $f = 2\text{GHz}$. In order to show the disturbance in surrounding outer space, the plot range is larger (from -0.6m to 0.6m) in the right column.

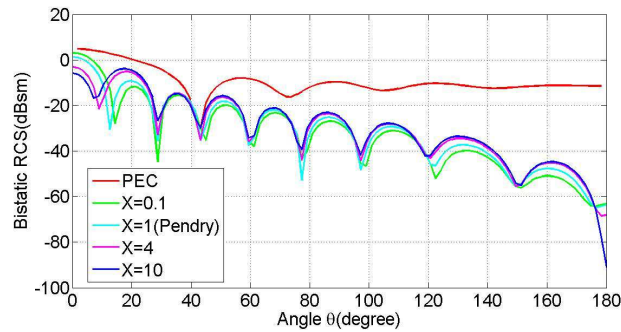


Fig. 8. Bistatic RCS of the concave-up nonlinear cloaks.

Table 1. The total scattering cross section (unit: dBsm) for concave-up nonlinearly transformed spherical cloaks ($x = 4$) under various segmentations in physical space.

$r_n(x)$ in Eq. (13)	$r_n(1)$	$r_n(2)$	$r_n(4)$	$r_n(6)$	$r_n(10)$
$r'(4)$ in Eq. (11)	-3.3	-3.5	-18.9	-3.8	-3.1

. * Note that $r_n(1)$ for concave-up cloaks corresponds to the case of equally dividing the physical space.

$r'(4)$, e.g., the sets of $x = 1$ ($r_n(1)$), $x = 2$ ($r_n(2)$), $x = 6$ ($r_n(6)$) and $x = 10$ ($r_n(10)$). The total cross sections corresponding to those four sets are compared with the best segmentation set of its own $r_n(4)$, i.e., equally dividing the virtual space of $x = 4$ into 40 initial-layers and then projecting onto physical space. We find that, for concave-up class $x = 4$, $r_n(4)$ is indeed its optimal segmentation among these possibilities.

5. Conclusion

In this paper, we discussed two novel classes of nonlinear-transformation-based spherical cloaks. An approximation mechanism for such classes of spherical cloaks by concentric isotropic sub-layers is proposed. The optimal segmentation in the virtual space is presented, and the role of nonlinearity in the coordinate transformation is discussed in order to provide better invisibility performance for the proposed classes of nonlinear spherical cloaks in both the near and far field. We find that concave-up nonlinear-transformation spherical cloaks exhibit better and more stable invisibility performance than the corresponding segmentation of linear-transformation or concave-down cloaks. An interesting topic for future exploration would be to consider a wider class of segmentation schemes, for example by using the segmentation presented here as the starting point for a numerical optimization (e.g., Ref. [28] for cylindrical cloaks) of variable segment thicknesses and material parameters.

6. Acknowledgement

This research was supported in part by the Army Research Office through the Institute for Soldier Nanotechnologies under Contract No. W911NF-07-D-0004.

Spherical cloaking using nonlinear transformations for improved segmentation into concentric isotropic coatings

Cheng-Wei Qiu^{1,2}, Li Hu², Baile Zhang¹, Bae-Ian Wu¹, Steven G. Johnson³, and John D. Joannopoulos¹

¹*Research Laboratory of Electronics, Massachusetts Institute of Technology, Cambridge, Massachusetts 02139, USA*

cwq@mit.edu

joannop@mit.edu

²*Department of Electrical and Computer Engineering, National University of Singapore, 4 Engineering Drive 3, Singapore 117576.*

³*Department of Mathematics, Massachusetts Institute of Technology, Cambridge, Massachusetts 02139, USA*

Abstract: Two novel classes of spherical invisibility cloaks based on nonlinear transformation have been studied. The cloaking characteristics are presented by segmenting the nonlinear transformation based spherical cloak into concentric isotropic homogeneous coatings. Detailed investigations of the optimal discretization (e.g., thickness control of each layer, nonlinear factor, etc.) are presented for both linear and nonlinear spherical cloaks and their effects on invisibility performance are also discussed. The cloaking properties and our choice of optimal segmentation are verified by the numerical simulation of not only near-field electric-field distribution but also the far-field radar cross section (RCS).

© 2018 Optical Society of America

OCIS codes: (290.5839) Scattering, invisibility; (160.1190) Materials: Anisotropic optical materials; (230.3205) Invisibility cloaks

References and links

1. J. B. Pendry, D. Schurig, and D. R. Smith, "Controlling electromagnetic fields," *Science* **312**, 1780 (2006).
2. D. Schurig, J. B. Pendry, and D. R. Smith, "Calculation of material properties and ray tracing in transformation media," *Opt. Express* **14**, 9794-9804 (2006). U. Leonhardt,
3. U. Leonhardt, "Optical conformal mapping," *Science* **312**, 1777-1780 (2006).
4. D. Schurig, J. B. Pendry, and D. R. Smith, "Transformation-designed optical elements," *Opt. Express* **15**, 14772-14782 (2007).
5. A. Greenleaf, M. Lassas, and G. Uhlmann, "Anisotropic conductivities that cannot be detected by EIT," *Physiol. Meas.* **24**, 413-419 (2003).
6. H. Chen and C. T. Chan, "Acoustic cloaking in three dimensions using acoustic metamaterials," *Appl. Phys. Lett.* **91**, 183518 (2007).
7. H. Chen, B. I. Wu, B. Zhang, and J. A. Kong, "Electromagnetic Wave Interactions with a Metamaterial Cloak," *Phys. Rev. Lett.* **99**, 063903 (2007).
8. B. Zhang, H. Chen, B. I. Wu, and J. A. Kong, "Extraordinary Surface Voltage Effect in the Invisibility Cloak with an Active Device Inside," *Phys. Rev. Lett.* **100**, 063904 (2008).

9. M. Rahm, D. Schurig, D. A. Roberts, S. A. Cummer, and D. R. Smith, "Design of electromagnetic cloaks and concentrators using form-invariant coordinate transformations of Maxwell's equations," *Photonics Nanostruc. Fundam. Appl.* **6**, 87 (2008).
 10. D. Kwon and D. H. Werner, "Two-dimensional eccentric elliptic electromagnetic cloaks," *Appl. Phys. Lett.* **92**, 013505 (2008).
 11. W. X. Jiang, T. J. Cui, G. X. Yu, X. Q. Lin, Q. Cheng and J. Y. Chin, "Arbitrarily elliptical cylindrical invisible cloaking," *J. Phys. D: Appl. Phys.* **41**, 085504 (2008).
 12. M. Yan, Z. Chao, and M. Qiu, "Cylindrical invisibility cloak with simplified material parameters is inherently visible," *Phys. Rev. Lett.* **99**, 233901 (2007).
 13. M. Yan, Z. Chao, and M. Qiu, "Scattering characteristics of simplified cylindrical invisibility cloaks," *Opt. Express* **15**, 17772C17782 (2007).
 14. H. Ma, S. B. Qu, Z. Xu, J. Q. Zhang, B. W. Chen, and J. F. Wang, "Material parameter equation for elliptical cylindrical cloaks," *Phys. Rev. A* **77**, 013825 (2008).
 15. W. Cai, U. K. Chettiar, A. V. Kildishev, and V. M. Shalaev, "Optical cloaking with metamaterials," *Nat. Photonics* **1**, 063904 (2007).
 16. B. Zhang, H. Chen, and B. I. Wu, "Limitations of high-order transformation and incident angle on simplified invisibility cloaks," *Opt. Express* **16**, 5445-5452 (2008).
 17. D. Schurig, J. J. Mock, B. J. Justice, S. A. Cummer, J. B. Pendry, A. F. Starr, and D. R. Smith, "Metamaterial electromagnetic cloak at microwave frequencies," *Science* **314**, 977 (2006).
 18. R. Liu, C. Ji, J. J. Mock, J. Y. Chin, T. J. Cui, and D. R. Smith, "Broadband Ground-Plane Cloak," *Science* **323**, 366-369 (2009).
 19. W. X. Jiang, J. Y. Chin, Z. Li, Q. Cheng, R. Liu, and T. J. Cui, "Analytical design of conformally invisible cloaks for arbitrarily shaped objects," *Phys. Rev. E* **77**, 066607 (2008).
 20. H. Ma, S. Qu, Z. Xu, and J. Wang, "Numerical method for designing approximate cloaks with arbitrary shapes," *Phys. Rev. E* **78**, 036608 (2008).
 21. A. Nicolet, F. Zolla, and S. Guenneau, "Electromagnetic analysis of cylindrical cloaks of an arbitrary cross section," *Opt. Lett.* **33**, 1584 (2008).
 22. C. W. Qiu, L. W. Li, T. S. Yeo, and S. Zouhdi, "Scattering by rotationally symmetric anisotropic spheres: Potential formulation and parametric studies," *Phys. Rev. E* **75**, 026609 (2007).
 23. W. Cai, U. K. Chettiar, A. K. Kildishev, G. W. Milton, and V. M. Shalaev, "Non-magnetic cloak without reflection," arXiv:0707.3641v1.
 24. R. Weder, "A rigorous analysis of high-order electromagnetic invisibility cloaks," *J. Phys. A: Math. Theor.* **41**, 065207 (2008).
 25. C. W. Qiu, L. W. Li, Q. Wu, and T. S. Yeo, "Field representations in general gyrotropic media in spherical coordinates," *IEEE Antennas Wirel. Propagat. Lett.* **4**, 467-470 (2007).
 26. C. W. Qiu, S. Zouhdi, and A. Razolek, "Modified spherical wave functions with anisotropy ratio: Application to the analysis of scattering by multilayered anisotropic shells," *IEEE Trans. Antennas Propagat.* **55**, 3515-3523 (2007).
 27. J. C. E. Sten, "DC fields and analytical image solutions for a radially anisotropic spherical conductor," *IEEE Trans. Dielect. Elec. Insul.* **2**, 360-367 (1995).
 28. B. I. Popa and S. A. Cummer, "Cloaking with optimized homogeneous anisotropic layers," *Phys. Rev. A* **79**, 023806 (2009).
 29. C. W. Qiu, L. Hu, L. Gao, "Trade-off between forward and backward scatterings of Linear and Nonlinear Spherical Invisibility Cloaks," *Progress In Electromagnetics Research*, to be submitted (2009).
-

1. Introduction

The use of coordinate transformation to control electromagnetic fields [1] has been receiving extensive attention [2, 3, 4]. This approach was generalized from the cloaking of thermal conductivity [5], and was further widely applied in electromagnetics and acoustics [1, 6], which provides new ways to conceal passive/active objects [7, 8] within their interiors invisible to external illuminations. The fundamental idea is that Maxwell's equations are invariant under a coordinate transformation if the material properties (electric permittivity and magnetic permeability) are altered appropriately; i.e., a specific spatial compression is equivalent to a variation of the material parameters in flat (original) space. Cloaks in regular shapes (e.g., spherical [1], square [9], cylindrical [10], or elliptic [11]) have been proposed based on the construction of explicit transformation matrices. There are many works devoted to the investigation of 2D cylindrical/elliptic cloaks approximated by, for example, simplified material parameters or equations [12, 13, 14, 15], or designed for limited incident angles [16]. Experimental investigations of 2D

cloaks have demonstrated significant reductions in the scattering cross section, albeit for narrow bandwidths in the microwave regime and for objects at most a few wavelengths in diameter so far [17]. Broader bandwidths have been demonstrated for cloaking an object on a ground plane, but again only for a few wavelengths diameter [18]. To design irregularly shaped cloaks, both analytical [19] and numerical methods [20, 21] have been proposed. In what follows, we will confine our discussion within the area of 3D electromagnetic spherical cloaks.

Inspired by the classic spherical cloak [1] based on a linear coordinate transformation, the expressions of electromagnetic fields were explicitly presented in terms of spherical Bessel functions along the lines of Mie scattering theory [7], and it again was demonstrated that the external incident wave cannot interact with the cloaked object in a perfect spherical cloak. Linear coordinate transformations correspond to a transverse/radial permittivity ratio (*anisotropy ratio* [22]) $\epsilon_t/\epsilon_r = r^2/(r - R_1)^2$, where R_1 is the radius of the cloaked region. The subtle point of the singularity in the coordinate transformation at the inner surface of the cloak was analytically shown to correspond to surface voltages [8] in spherical cloaks, leading to an explicit physical explanation for why the wave cannot leave the cloaked region and external waves cannot enter that region. These works on spherical cloaks considered linear coordinate transformations, while more recently nonlinear (“high-order”) transformations have been considered in order to obtain more degrees of freedom in designing the material parameters [23, 24]. In this paper, we consider the utility of nonlinear coordinate transformations to improve the performance of the cloak when it is approximated (segmented) into a sequence of piecewise-homogeneous layers. If the anisotropy ratio differs from $r^2/(r - R_1)^2$, it will lead to quite complicated formulations for the field expressions, which cannot be treated by the previous method for a position-dependent anisotropy ratio [7] or by the method for a constant anisotropy ratio [25, 26]. Here, in order to study the proposed nonlinear-transformation spherical cloaks, each anisotropic cloaking shell is discretized into multiple alternating homogeneous isotropic coatings, not only for the ease of fabrication but also for the computation convenience in dealing with arbitrary anisotropy ratios.

In general, practical implementations of passive invisibility cloaks by coordinate transformation are limited by several factors, in addition to the bandwidth limitations (from material dispersion) mentioned above. First, there are fabrication imperfections and the finite size of the subwavelength components of the metamaterials. Second, there is material absorption, which is especially challenging when an extreme resonant response is required of the material in order to obtain very large or very small permittivity/permeability. Third, there is the difficulty of fabricating continuously varying anisotropic materials. In this paper, we focus only on the third issue. A common approximation for continuously varying materials is to segment them into piecewise-homogeneous layers, and we show that the choice of coordinate transformation has a significant impact upon the success of this approximation. We argue that the segmentation is best performed in virtual space rather than in the physical (transformed) coordinates. We also demonstrate that the anisotropic materials can be further approximated by a sequence of isotropic-material layers. The optimal selection of material parameters, nonlinear transformation, and segmentation (in virtual space), in order to achieve a low scattering cross section over a wide range of observation angles, is found for nonlinear spherical cloaks and verified by numerical results.

2. Preliminaries

The configuration of the spherical cloaking structure is shown in Fig. 1. The inner region ($r < R_1$) is a perfect electric conductor (PEC) and the intermediate region ($R_1 < r < R_2$) is filled by the nonlinearly transformed spherical cloak, characterized by $\bar{\epsilon}(r)$ and $\bar{\mu}(r)$, which will be discussed below. The electric field is polarized along the x axis and propagating along the z axis.

By applying the decomposition method and separation of variables [22], the equation for the

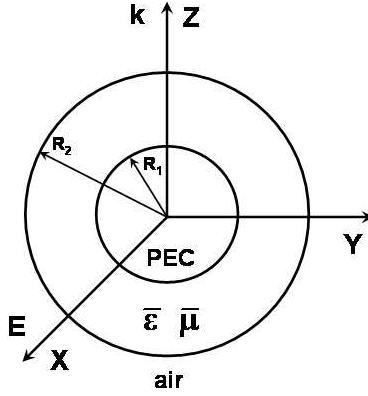


Fig. 1. The geometry of a spherical cloaking structure.

radial component of the field potentials becomes

$$\left\{ \frac{\partial^2}{\partial r^2} + \left[k_r^2 - A_{e,m} \frac{n(n+1)}{r^2} \right] \right\} f(r) = 0, \quad (1)$$

where the subscripts e and m denote the electric and magnetic anisotropic ratio, respectively, and $k_r = \omega \sqrt{\bar{\mu}_r \bar{\epsilon}_r}$ [22]. For $\bar{\epsilon}$ and $\bar{\mu}$ of perfect linear spherical cloaks [1], i.e., $A_e = A_m = r^2/(r - R_1)^2$, Eq. (1) is reduced to

$$\left\{ \frac{\partial^2}{\partial r^2} + \left[k_r^2 - \frac{n(n+1)}{(r - R_1)^2} \right] \right\} f(r) = 0. \quad (2)$$

Thus, the radial component $f(r)$ can be solved in a way similar to that for isotropic materials, except for the change in the argument of resultant Bessel/Hankel functions. However, given a set of $\bar{\epsilon}$ and $\bar{\mu}$ derived from a certain transform, the anisotropy ratio may not be $r^2/(r - R_1)^2$ anymore, and then the radial component cannot be solved explicitly in the same way. In this situation, we could approximate the original inhomogeneous anisotropic cloak by many thin, homogeneous anisotropic coatings, and the diffraction problem can thus be solved in terms of analytical Bessel/Hankel functions satisfying boundary conditions at each interface. Nevertheless, the requirement of anisotropic materials still remains. Alternatively, to further alleviate the restriction in material complexity, the original inhomogeneous anisotropic cloaking materials can be approximated by the limit of many thin, concentric, homogeneous, *isotropic* coatings, forming an effective anisotropic medium, which will be discussed in this section.

First, we consider a general spherical cloak characterized by $\bar{\epsilon} = \epsilon_r(r) \hat{r}\hat{r} + \epsilon_t(r) (\hat{\theta}\hat{\theta} + \hat{\phi}\hat{\phi})$ and $\bar{\mu} = \mu_r(r) \hat{r}\hat{r} + \mu_t(r) (\hat{\theta}\hat{\theta} + \hat{\phi}\hat{\phi})$, in which $\epsilon_r(r) = \mu_r(r)$ and $\epsilon_t(r) = \mu_t(r)$ are position-dependent in general. It is then divided into M initial-layers (anisotropic) but the thickness of individual initial layers may or may not be identical, depending on the transformation. Given a coordinate transformation function $r' = f(r)$ between the virtual space (i.e., $\Omega'(r'), 0 < r' < R_2$) and the compressed space (i.e., $\Omega(r), R_1 < r < R_2$), the stepwise segmentation in physical space (r) is desired to mimic the transformation function as well as possible and we also desire that the segmentation not be too complicated. We find that equally dividing the *virtual* space (r') into M initial-layers will make the segmentation on the physical space (r) “self-adaptive” in a simple way—it automatically uses a finer discretization in regions of physical space where the anisotropic materials are varying more rapidly—which will result in better invisibility perfor-

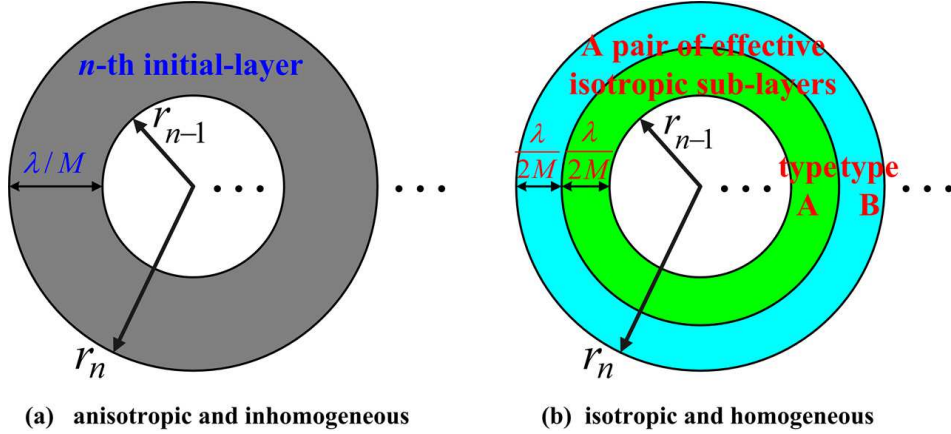


Fig. 2. The discretization of a general anisotropic spherical cloak (a) into an equivalent isotropic coated structure (b). An illustrative example for the conversion from the n -th anisotropic initial-layer (width is $r_n - r_{n-1}$) into its two sub-layers (isotropic) with equal thickness $(r_n - r_{n-1})/2$ has been shown.

mance. This conversion is illustrated in Fig. 2. Throughout this paper, we apply the same condition, i.e., the segmented layers in r' are of equal thickness, which represents a good choice of segmentation in the initial-layers in the cloak shell $R_1 < r < R_2$. By projecting the segmentation in $r'_n = R_2 \cdot n/M$ onto the physical r , one has $r_n = f^{-1}(r'_n)$, ($n=1, 2, \dots, M$). Thus, the geometry of every initial-layer in Fig. 2(a) is determined.

Subsequently, we mimic each spherically anisotropic initial layer by a pair of effective isotropic sub-layers (type-A and type-B) with equal thickness at $(r_n - r_{n-1})/2$, as shown in Fig. 2(b). The material parameters of type-A and type-B isotropic dielectrics can be inferred and derived from the result for radial conductivity by Sten [27]:

$$\epsilon_A = \mu_A = \epsilon_t + \sqrt{\epsilon_r^2 - \epsilon_t \epsilon_r} \quad (3a)$$

$$\epsilon_B = \mu_B = \epsilon_t - \sqrt{\epsilon_r^2 - \epsilon_t \epsilon_r}. \quad (3b)$$

Now, the original spherical cloak turns to be a concentric isotropic coatings. Throughout this paper, $M = 40$ and $R_2 = 2R_1 = 2\lambda$ are chosen in order that the validity of Eq. (3) can be maintained, i.e., sub-layers have to be sufficiently thin. Alternatively one could also choose a smaller M associated with the corresponding parameters determined by optimization methods and then subdivide each anisotropic layer into many more than two isotropic sub-layers.

When converting the n -th initial layer into its pair of effective isotropic sub-layers, we need to pick a specific radial position for those ϵ_r and ϵ_t on the right-hand side of Eq. (3) within the initial layer in order to determine corresponding parameters of the two isotropic dielectrics (ϵ_A, μ_A) and (ϵ_B, μ_B) on the left-hand side of Eq. (3) and in Fig. 2(b). According to [29], such a discretization mechanism using $r = r_n$ in Eq. (3) for the n -th initial layer will give a good compromise for both forward and backward scatterings, while retaining good invisibility performance.

3. Effects of Nonlinear Transformation in Nonlinear Spherical Cloaks

Pendry's spherical cloak [1] is a linear one, and hence it is a straight line if one plots the transformation function r' against the physical radius r . In what follows, we introduce two classes

of nonlinear-transformation spherical cloaks, and we discuss how to restore and improve the invisibility performance after discretization by choosing a proper nonlinear transformation and by choosing a suitable compensation scheme while discretizing the original spherical cloak into multilayer isotropic structures. The two types of spherical cloaks considered here are classified in terms of the negative (i.e., concave-down) or positive (i.e., concave-up) sign of the second derivative of the transformation function. It is important to reiterate that all three designs—linear, concave-up, and concave-down—are perfect cloaks for the exact inhomogeneous design, and we are only considering the breakdown of invisibility when the design is discretized into homogeneous layers.

3.1. Concave-Down Nonlinear Transformation

To compress a sphere of air at the radius R_2 in Ω' (original) space into a shell at the region $R_1 < r < R_2$ in Ω (compressed) space, we propose a class of prescribed functions

$$r'(x) = \frac{R_2^{x+1}}{R_2^x - R_1^x} \left[1 - \left(\frac{R_1}{r} \right)^x \right] \quad (4)$$

where x denotes the degree of the nonlinearity in the transformation. When x is very small in Eq. (4), the curves are difficult to distinguish and all approach to the same limiting case when $x \rightarrow 0$:

$$r'(x) = \frac{R_2 \text{Ln}[r/R_1]}{\text{Ln}[R_2/R_1]}. \quad (5)$$

Thus the parameters $\bar{\epsilon}$, $\bar{\mu}$ in the transformed coordinates can be written in term of $\bar{\epsilon}'$, $\bar{\mu}'$ in the original space by

$$\bar{\epsilon}(r) = A \bar{\epsilon}'(r') A^T / \det(A), \quad \bar{\mu}(r) = A \bar{\mu}'(r') A^T / \det(A) \quad (6)$$

where A is the Jacobian matrix with elements defined as $A_{ki} = \partial r_k / \partial r'_i$.

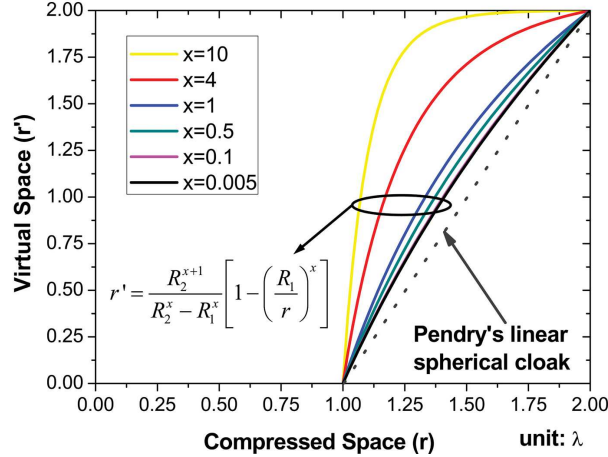


Fig. 3. The concave-down nonlinear transformation. When $x < 0.1$, all mapping curves are overlapping, meaning they effectively lead to the same performance. When x becomes large, the curve will nearly become a step function over $1\lambda < r < 2\lambda$.

Note that all curves belonging to those transformation functions in Eq. (4) have negative second derivative with respect to the physical space r , and we term this class of transformations

the *concave-down* nonlinear transformation. The nonlinear transformation function in Eq. (4) only depends on the radial component r in the spherical coordinate system (r, θ, ϕ) . Thus it is easy to find that the Jacobian matrix A is diagonal. Considering that the original space is filled with air ($\bar{\boldsymbol{\epsilon}} = \bar{\boldsymbol{\mu}} = 1$), Eq. (6) can be rewritten as

$$\bar{\boldsymbol{\epsilon}} = \bar{\boldsymbol{\mu}} = \text{diag}[\lambda_r^2, \lambda_\theta^2, \lambda_\phi^2] / \lambda_r \lambda_\theta \lambda_\phi = \text{diag}\left[\frac{\lambda_r}{\lambda_\theta \lambda_\phi}, \frac{\lambda_\theta}{\lambda_r \lambda_\phi}, \frac{\lambda_\phi}{\lambda_r \lambda_\theta}\right] \quad (7)$$

where

$$\lambda_r = \frac{\partial r}{\partial r'} = \frac{(R_2^x - R_1^x)r^{x+1}}{xR_1^x R_2^{x+1}} \quad (8a)$$

$$\lambda_\theta = \lambda_\phi = \frac{r}{r'} = \frac{(R_2^x - R_1^x)r^{x+1}}{R_2^{x+1}(r^x - R_1^x)} \quad (8b)$$

denoting three principal stretches of the Jacobian matrix. Finally, the desired parameters in the compressed space ($R_1 < r < R_2$) are shown to be

$$\epsilon_r = \mu_r = \frac{R_2^{x+1}(r^x - R_1^x)^2}{xR_1^x(R_2^x - R_1^x)r^{x+1}} \quad (9a)$$

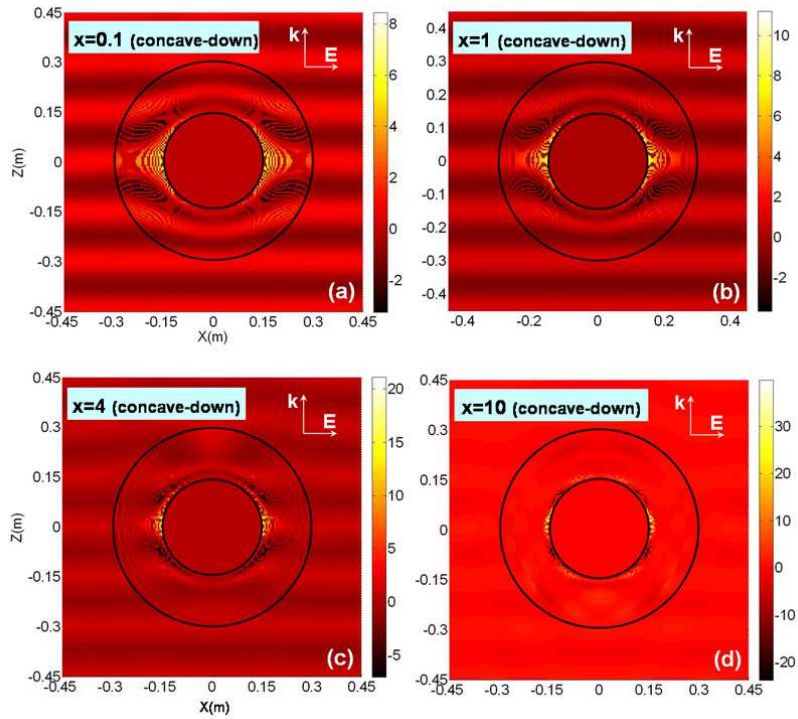
$$\epsilon_\theta = \mu_\theta = \epsilon_\phi = \mu_\phi = \frac{xR_1^x R_2^{x+1}}{(R_2^x - R_1^x)r^{x+1}}. \quad (9b)$$

Given such radial and transversal parameters, it is obvious that Eq. (1) cannot be simply solved due to the complicated anisotropy ratio $A_{e,m} = \epsilon_t / \epsilon_r = x^2 R_1^{2x} / (r^x - R_1^x)^2$ in our current case. In addition, one can also find that when the virtual space is equally discretized using a concave-down nonlinear transformation, the segmentation of the initial layers in Fig. 2 in the physical space r is

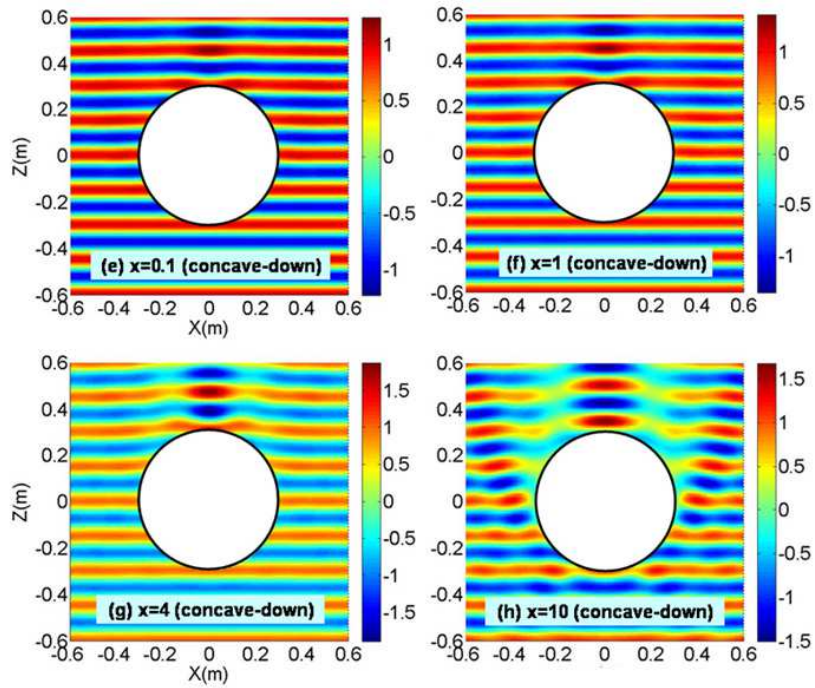
$$r_n(x) = \left[1 - \frac{R_2^x - R_1^x}{R_2^x} \frac{n}{M}\right]^{-1/x} \cdot R_1, \quad n=1, 2, \dots, M. \quad (10)$$

Here, we will study the effects of the nonlinear factor x in the near-field and far-field of the discretized nonlinear-transformation spherical cloaks. We fix $M=40$, and consider the cases of $x=0.1$, $x=1$, $x=4$, and $x=10$ in concave-down nonlinear cloaks, shown in Fig. 4. It can be seen from Figs. 4(a-d) that when x increases, the magnitude of electric field increases significantly inside the cloak. This is because more energy is guided towards the inner boundary of the PEC core, which in turn makes the cloaked PEC more *visible* to external incidences. To prove that the large electric fields only occur in the region $R_1 < r < R_2$ and to study the effect of x on individual near-field perturbations more explicitly, only the fields outside the cloak are presented in Figs. 4(e-f). One can again confirm that, for discretized concave-down nonlinear spherical cloaks, smaller x leads to smaller disturbance in electric fields in the outer space. In particular, the degradation in the invisibility in the forward direction is proportional to the value of x (see Fig. 4(g) and Fig. 4(h)).

In Fig. 5, we consider the far fields of those cases of Fig. 4. For comparison purposes, we introduce two more curves, PEC and Pendry's cloak. It should be noted that the curve corresponding to Pendry's cloak is a straight line, and the same segmentation procedure as discussed above is applied to it, which is the same as equally dividing it into M initial-layers in the physical space (see Fig. 3). From Fig. 5, it can be seen that for concave-down nonlinear transformations, the cloaking property is better retained when x is small. Except for the forward direction,



$\text{Re}[E_{\text{total}}]$ in all regions on x - z plane



$\text{Re}[E_{\text{total}}]$ outside the cloak on x - z plane

Fig. 4. Near-field interaction in the presence of the proposed nonlinear spherical cloak with different values of x for the concave-down class. The inner region $0 < r < R_1$ is filled by PEC. M is set to be 40. Frequency is 2GHz. The total electric fields are plotted only in the region $r > R_2$ in (e-h).

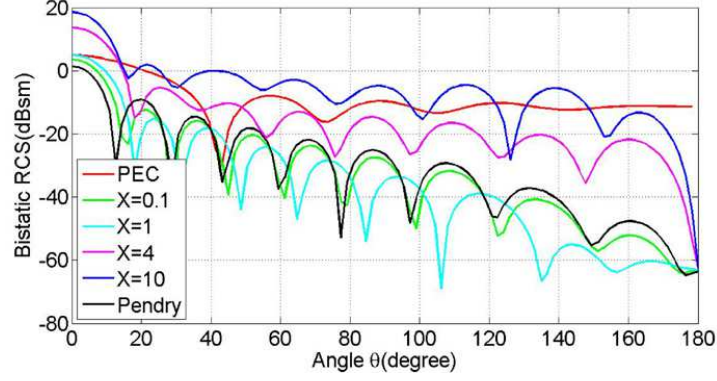


Fig. 5. Bistatic RCS of the concave-down nonlinear cloaks. $M = 40$.

concave-down nonlinear transformation with small x can achieve even lower RCS over a wide range of observation angles. As x keeps increasing, their RCSs are increasing dramatically and can be larger than that of a uncloaked PEC core (e.g., $x = 10$). No matter how large x becomes, the suppressed backward scattering is still maintained [7] though it is not exactly zero due to the discretization, but the forward scattering will become higher and higher, which is not desired in the cloaking application. Those far-field characteristics are consistent with the perturbation in corresponding near-field patterns in Fig. 4.

3.2. Concave-Up Nonlinear Transformation

We can also propose another class of prescribed functions

$$r'(x) = \frac{R_2 R_1^x}{R_2^x - R_1^x} \left[\left(\frac{r}{R_1} \right)^x - 1 \right]. \quad (11)$$

It is found that when $x \rightarrow 0$, it also approaches to the same limit as Eq. (5). In the same manner, we can obtain the desired parameters in the compressed space ($R_1 < r < R_2$)

$$\varepsilon_r = \mu_r = \frac{R_2 (r^x - R_1^x)^2}{x (R_2^x - R_1^x) r^{x+1}} \quad (12a)$$

$$\varepsilon_\theta = \mu_\theta = \varepsilon_\phi = \mu_\phi = \frac{x R_2 r^{x-1}}{R_2^x - R_1^x}. \quad (12b)$$

Note that the case $x = 1$ is exactly Pendry's linear spherical cloak.

It can be seen in Fig. 6 that all curves belonging to Eq. (11) have positive second derivatives, and we term this class of transformations as the *concave-up* nonlinear transformations. Also, it is found that the limiting case of Eq. (5), i.e., $x \rightarrow 0$, is the dividing line between the concave-down and concave-up classes. Since $x \ll 1$ in Eq. (11) is actually very close to the situation of $x \ll 1$ for concave-down nonlinear transformations, we will not revisit that case here. Instead, we only consider $x = 1$, $x = 4$, and $x = 10$ concave-up transformations [Eq. (12)], and the segmentation for concave-up nonlinear spherical cloaks in physical space r turns out to be

$$r_n(x) = \left[\frac{R_2^x - R_1^x}{R_1^x} \frac{n}{M} + 1 \right]^{1/x} \cdot R_1, \quad n=1, 2, \dots, M. \quad (13)$$

We are interested to see which class will give rise to better invisibility performance, after discretization, if all the other conditions are the same. We still plot the near field of concave-up cloaks at “ $x=1$ ”, “ $x=4$ ”, and “ $x=10$ ”. Comparing Fig. 4 with Fig. 7, one can see that: (1)

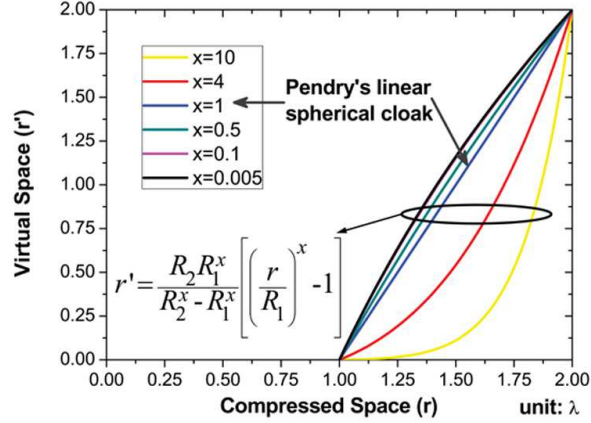


Fig. 6. The concave-up nonlinear transformation. When $x = 1$, it is exactly Pendry's linear cloak, which can be verified by inserting $x = 1$ into Eq. (12). When x gets extremely large, the mapping curve will nearly become a sharp impulse when $r \rightarrow 2\lambda$.

the peak amplitude of the electric field is proportional to x in both classes; (2) for each value of x , concave-up transformation cloaks have lower peak amplitudes than concave-down transformation cloaks, i.e., the perturbation inside the cloak region is smaller; (3) the perturbation outside the cloak of concave-up transformation cloaks is also lower than that of concave-down transformation cloaks in all cases of x ; (4) the invisibility performance is better maintained for concave-up transformations even when $x = 10$ or even larger. Hence, spherical cloaks based on concave-up nonlinear transformations exhibit better invisibility after discretization.

Fig. 8 exhibits some interesting features which distinguish it from the far fields of concave-down transformations in Fig. 5. Over a wide range of angles, the invisibility performance of spherical cloaks based on concave-up nonlinear transformations are more stable under variations in x . More importantly, when x increases (e.g., $x = 4$ or $x = 10$), though the RCS will be a bit larger than Pendry's linear cloak at most angles, the RCS near the forward direction will be reduced greatly compared with that of classic linear cloak. Such far-field phenomena are also connected with the near-field patterns. It is important to point out that the increase of x in concave-up transformations [see Figs. 7(a-c)] will push the "hot" areas (where the electric field is very high) further and further away from the spherical PEC core, so the induced shadow and the far-field pattern become stable with increasing x . However, the increase of x in the concave-down transformations has little effect in shifting away the "hot" positions from the core [see Fig. 4(a-d)], which results in larger interaction with the PEC core. Hence, the RCS reduction in the far field is degraded with the increase of x in the concave-down class as shown in Fig. 5.

4. Justification of Improved Segmentation

It has been pointed out that usually we require a large value of M during the discretization process, otherwise the conversion scheme in Fig. 2 will lose its accuracy. We also find that a nonlinear transformation with a given x of its concave-up class will yield a better invisibility by taking the segmentation as Eq. (13) in the physical space (this is also the only way to determine sub-layers of type-A and type-B dielectrics in practice). Here the justification is given. The concave-up class with $x = 4$, which is characterized by the mapping curve $r'(4) = \frac{R_2 R_1^4}{R_2^4 - R_1^4} \left[(r/R_1)^4 - 1 \right]$, is considered as an example.

In Table I, different segmentation $r_n(x)$ sets (see Eq. 13) for real radius r are applied to

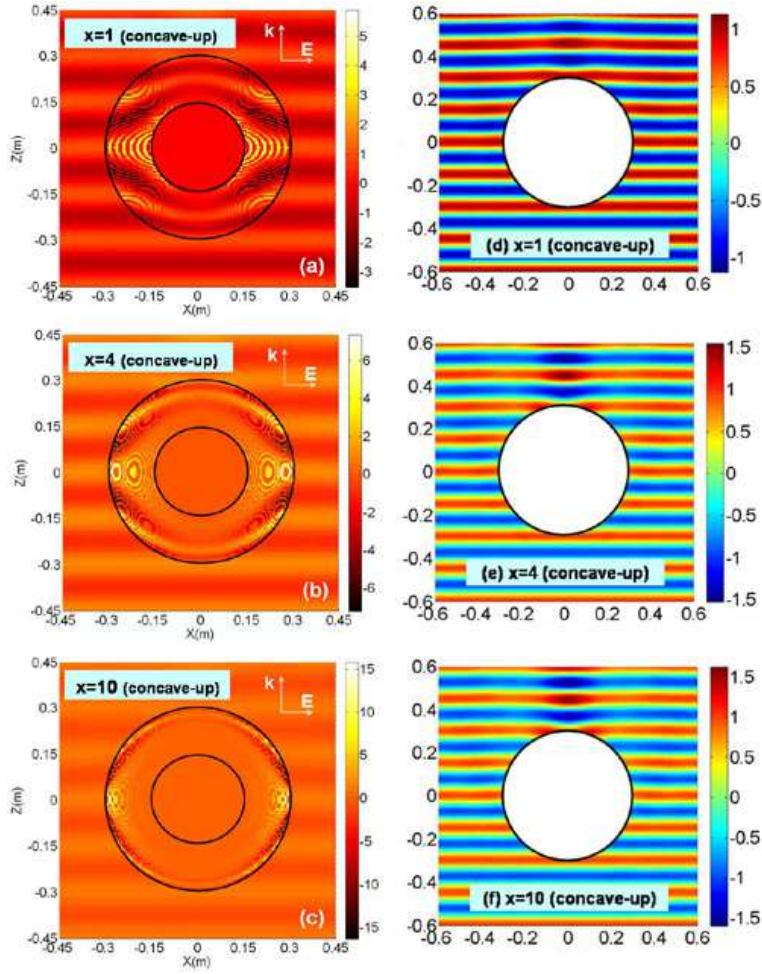


Fig. 7. $\text{Re}[E_{\text{total}}]$ on x - z plane for the proposed concave-up nonlinear transformation cloaks at $x = 1$, $x = 4$ and $x = 10$, respectively. Figs. 7(a-c) present total electric fields in all areas while Figs. 7(e-f) show the total fields only outside the cloak ($r > R_2$). $M = 40$ and $f = 2\text{GHz}$. In order to show the disturbance in surrounding outer space, the plot range is larger (from -0.6m to 0.6m) in the right column.

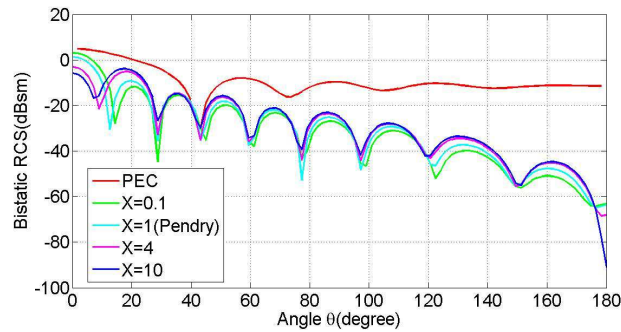


Fig. 8. Bistatic RCS of the concave-up nonlinear cloaks.

Table 1. The total scattering cross section (unit: dBsm) for concave-up nonlinearly transformed spherical cloaks ($x = 4$) under various segmentations in physical space.

$r_n(x)$ in Eq. (13)	$r_n(1)$	$r_n(2)$	$r_n(4)$	$r_n(6)$	$r_n(10)$
$r'(4)$ in Eq. (11)	-3.3	-3.5	-18.9	-3.8	-3.1

. * Note that $r_n(1)$ for concave-up cloaks corresponds to the case of equally dividing the physical space.

$r'(4)$, e.g., the sets of $x = 1$ ($r_n(1)$), $x = 2$ ($r_n(2)$), $x = 6$ ($r_n(6)$) and $x = 10$ ($r_n(10)$). The total cross sections corresponding to those four sets are compared with the best segmentation set of its own $r_n(4)$, i.e., equally dividing the virtual space of $x = 4$ into 40 initial-layers and then projecting onto physical space. We find that, for concave-up class $x = 4$, $r_n(4)$ is indeed its optimal segmentation among these possibilities.

5. Conclusion

In this paper, we discussed two novel classes of nonlinear-transformation-based spherical cloaks. An approximation mechanism for such classes of spherical cloaks by concentric isotropic sub-layers is proposed. The optimal segmentation in the virtual space is presented, and the role of nonlinearity in the coordinate transformation is discussed in order to provide better invisibility performance for the proposed classes of nonlinear spherical cloaks in both the near and far field. We find that concave-up nonlinear-transformation spherical cloaks exhibit better and more stable invisibility performance than the corresponding segmentation of linear-transformation or concave-down cloaks. An interesting topic for future exploration would be to consider a wider class of segmentation schemes, for example by using the segmentation presented here as the starting point for a numerical optimization (e.g., Ref. [28] for cylindrical cloaks) of variable segment thicknesses and material parameters.

6. Acknowledgement

This research was supported in part by the Army Research Office through the Institute for Soldier Nanotechnologies under Contract No. W911NF-07-D-0004.